A simple analytical model to accurately predict self-resonance frequencies of on-silicon-chip inductors in TEM mode and eddy current mode

Jyh-Chyurn Guo *, Teng-Yang Tan

Department of Electronics Engineering, National Chiao-Tung University No. 1001, Ta-Hsueh Road, Hsinchu 300, Taiwan, ROC

ABSTRACT

For the first time, a simple analytical model in the form of explicit formulas was derived for on-silicon-chip inductors. This analytical model can accurately calculate self-resonance frequencies (f_{SR}) in TEM mode and eddy current mode corresponding to very high and very low substrate resistivities (ρ_{Si}). Furthermore, this derived model can predict and explain the interesting result that f_{SR} keeps nearly a constant independent of ρ_{Si} in TEM and eddy current modes but is critically determined by the inductance and parasitic capacitances. The simple model is useful in on-silicon-chip inductor design for increasing f_{SR} under specified inductance target for broadband RF circuit design and applications.

© 2008 Elsevier Ltd. All rights reserved.

1. Introduction

On-Si-chip inductors have been the most critical components in Si CMOS RF integrated circuit (RFICs) design attributed to the advantages in high integration level, low fabrication cost, and performance. Unfortunately, the resistive loss in the metal coils and substrate loss through the semiconducting silicon emerge as two major factors responsible for quality factor (Q) degradation generally suffered by the on-Si-chip inductors [1,2]. The challenges to on-chip inductor design and performance improvement attract extensive research activities in aspects of materials, processes, structures, layouts, and operation schemes [3–8]. High resistivity substrate has been proposed and proven as an effective way to improve Q [5,6]. However, most of the effort was focused on the materials and processes for fabrication and very limited works were done on the development of Spice-compatible models, which can predict the substrate resistivity effect for high frequency circuit simulation.

In our recent work, electromagnetic (EM) simulation was carried out using the calibrated ADS momentum to explore the spiral inductor characteristics under varying substrate resistivities ($\rho_{Si} = 0.05–1\,K\,\Omega\,cm$) [9]. Three operation modes such as TEM, slow-wave, and eddy current modes first derived by Hasegawa et

al. for microstrip lines in Si–SiO$_2$ system, based on wave propagation analysis [10] can be reproduced for on-Si-chip spiral inductors using EM simulation. Interesting results are demonstrated in terms of maximum Q (Q_m) and f_{SR} corresponding to the three operation modes and match with what was reported by Burghartz and Rejaei [2].

Unfortunately, EM simulation generally requires extensive computation time and memory and is not suitable for circuit simulation, which demands a quick turn around in design. Moreover, the slow cycle time always restricts EM simulation to few inductors with specified geometries. Facing the challenges and demand, many equivalent circuit models were proposed for on-chip inductors in circuit simulation. However, most of them reveal critical limitations in bandwidth, scalability, and most importantly lacking consideration of substrate resistivity effects [11–15]. One of the lumped element models, based on quasi-static field analysis was presented for simulating substrate loss effect [16]. However, the comparison with measurement was limited to Re(Z_{in}) and $L = Im(Z_{in})$ in a narrow bandwidth within 10 GHz. The accuracy in terms of S-parameters (magnitude and phase), Re($-1/Y_{21}$), quality factor Q, and self-resonance frequency f_{SR} was not verified and the results under varying substrate resistivities were not demonstrated.

Due to the fact, a new inductor model in the form of lumped elements and named as T-model was then developed in our original work. This T-model incorporates important features of being suitable for circuit simulation with proven broadband accuracy,

* Corresponding author. Tel.: +886 3 5131368; fax: +886 3 5724361.
E-mail address: jcguo@mail.nctu.edu.tw (J.-C. Guo).

scalability, and most importantly the relevant correlation with ρ_{Si} for all model parameters [9]. In this paper, based on the proven T-model, simple analytical model equations can be derived to explain and predict the interesting result of f_{SR} presented in TEM and eddy current modes where the dependence on ρ_{Si} becomes very weak but the inductance and parasitic capacitances play a major role. The simple model in an analytical form of equivalent circuit elements can help guide on-Si-chip inductor design to increase f_{SR} under specified inductance target for broadband RF circuit design and applications.

2. Operation modes of varying substrate resistivities

EM simulation using Agilent ADS momentum with an extensive calibration on 0.13 μm Cu BEOL (back-end-of-line) technology parameters was conducted to explore the broadband characteristics of inductors under varying ρ_{Si}. The first subject is to verify the three operation modes predicted by wave propagation analysis done for microstrip lines in Si–SiO$_2$ system [10]. Afterward, analytical model equations will be derived through an equivalent circuit analysis on our T-model to calculate and explain the interesting results presented in f_{SR} under varying ρ_{Si}. At first, a rigorous benchmark between our T-model and conventional π-model is performed based on measured high frequency parameters to verify and justify the advantages of T-model over conventional π-model in mentioned features.

2.1. Lumped element models for inductor simulation – T-model and π-model

Fig. 1a and b illustrate the equivalent circuit schematics for the proposed T-model and π-model respectively. T-model in Fig. 1a incorporates two RLC networks representing spiral coils on the top and substrate at the bottom. Each RLC network consists of four circuit elements and is linked to each other through $C_{ox1,2}$ in series with parallel RL for simulating EM coupling between the spiral inductors and the lossy substrate underneath. The physical property defined for each element in the equivalent circuit can be referred to our previous publications [9]. As for π-model in Fig. 1b, there are one RLC network for the spiral coils above and a pair of parallel RC emulating the substrate below. Between the coil RLC and substrate RC, a pair of series LC ($C_{ox1,2}$ and $L_{sub1,2}$) serve as the coupling path. Note that there is no coupling between the pair of substrate RC in the conventional π-model.
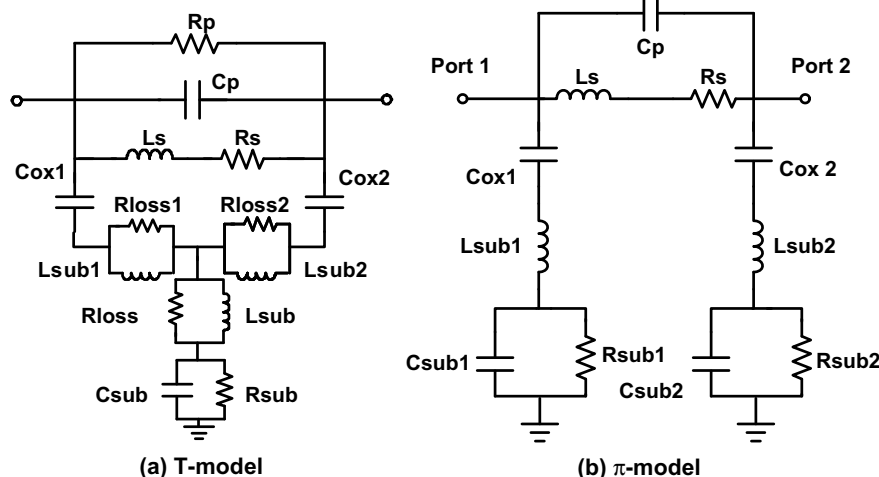
Fig. 2 indicates a good match between T-model and measurement in terms of S_{11}, S_{21}, $L(\omega) = \text{Im}(Z_{in}(\omega))$, $\text{Re}(Z_{in}(\omega))$, and $Q(\omega)$ for inductors on standard Si substrate with ρ_{Si} = 10 Ω cm, over a broad frequency to 20 GHz. Note that ADS momentum results are presented together for proving the EM simulation accuracy realized through an appropriate calibration. Regarding π-model, an acceptable accuracy can be achieved for S_{11} and Q but a significant deviation was suffered in other key parameters, such as S_{21}, $L(\omega)$, $\text{Re}(Z_{in}(\omega))$, and $\text{Re}(-1/Y_{21})$ over higher frequencies. Fig. 3a and b demonstrate a comparison between T-model, π-model, and measurement in which a dramatic deviation was revealed in S_{21} and $\text{Re}(-1/Y_{21})$ at higher frequencies beyond 10 GHz. The most critical error appears at $\text{Re}(-1/Y_{21})$, with an opposite trend with respect to the measurement, i.e. an exponential rising in π-model versus a fall-off in measurement (Fig. 3b). The apparent fall-off in measured $\text{Re}(-1/Y_{21})$ over high frequencies manifests a significant port-to-port coupling through the lossy substrate. Our T-model can simulate this substrate coupling effect with a reasonable accuracy whereas π-model presents an abnormal result and exposes its limitation. Lacking a coupling path between the pair of substrate RC circuits is considered the major cause responsible for the limitation. Interestingly, a similar observation and consistent comments on the intrinsic weakness of π-model can be referred to multiple literatures [13–15].

2.2. EM simulation for substrate resistivity effect in on-Si-chip inductors

EM simulation was performed using the calibrated ADS momentum for investigating substrate resistivity effect on inductors. Three operation modes such as TEM, slow-wave, and eddy current modes corresponding to a wide range of ρ_{Si} (0.05–1 K Ω cm) can be reproduced [2,9]. Fig. 4a and b present two key parameters, Q_m and f_{SR} as functions of ρ_{Si}. Interesting result is identified in the region of ρ_{Si} = 0.5–10 Ω cm where f_{SR} drops monotonically with reducing ρ_{Si} while Q_m reveals a hump due to an initial increase and then a fall-off with further reduction of ρ_{Si}. This drop of f_{SR} and increase of Q_m suggest that the spiral coil is getting into a resonator mode, i.e. slow-wave mode. As for high resistivity region with $\rho_{Si} > 10$ Ω cm, f_{SR} saturates at a maximum while Q_m increases continuously with ρ_{Si}. This region is so called TEM mode or inductor mode, which favors inductor operation with high Q attributed to suppressed resonance in substrate of dielectric property. Note that the saturation of f_{SR} under further increasing substrate resis-
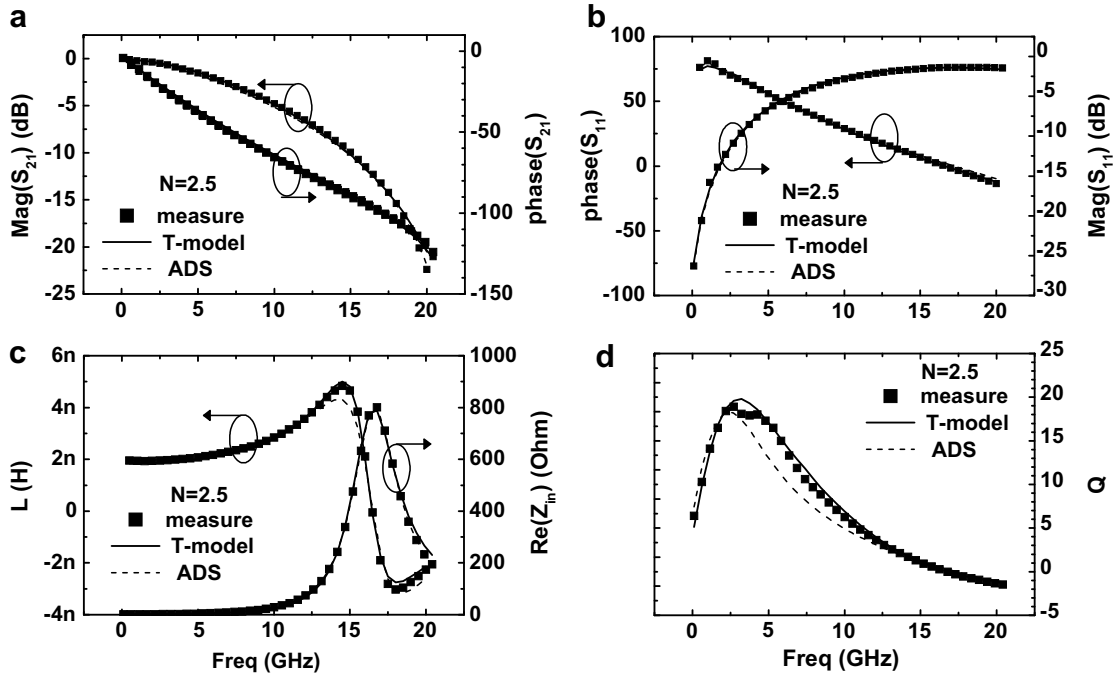

Fig. 1. Equivalent circuit schematics of lumped element models for on-chip spiral inductors: (a) T-model; (b) π-model.

Fig. 2. Comparison between ADS momentum simulation, measurement, and T-model for on-chip inductor: (a) S_{11}(magnitude, phase); (b) S_{21}(magnitude, phase); (c) $L(\omega)$, $Re(Z_{in}(\omega))$); (d) $Q(\omega)$. $\rho_{Si} = 10\ \Omega$ cm is defined for standard silicon substrate in the EM simulation.

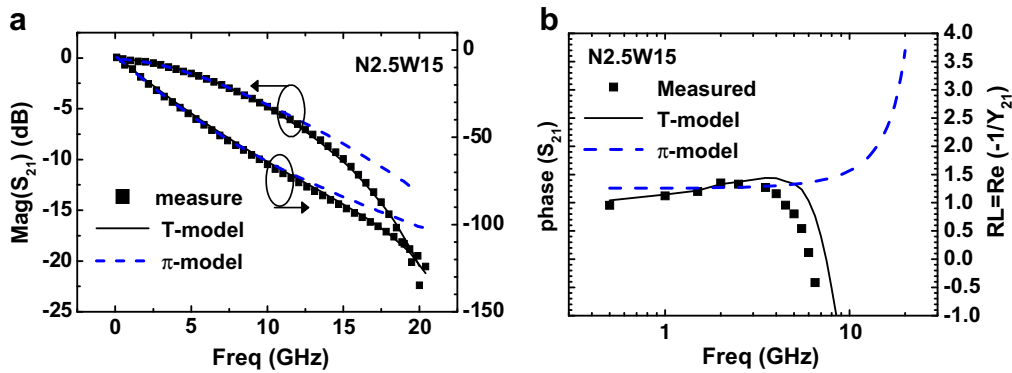**Fig. 3.** Comparison between T-model, π-model, and measurement in high frequency parameters (a) S_{11} (magnitude, phase) (b) $Re(-1/Y_{21})$ for on-chip inductor.
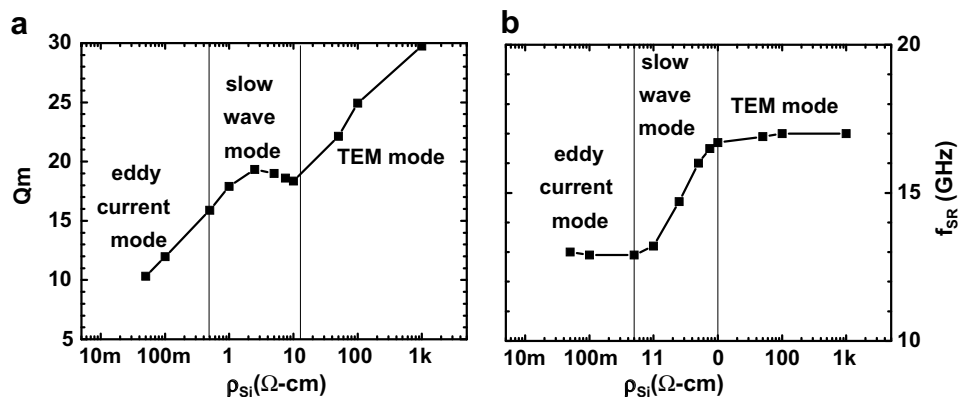

Fig. 4. ADS momentum simulation for prediction of: (a) Q_m; (b) f_{SR} under varying substrate resistivities, $\rho_{Si} = 0.05$–1 K Ω cm.

tivities beyond the standard Si, i.e. $\rho_{Si} > 10\ \Omega$ cm can be supported by the experimental results published in 2003 IEDM [6] in which ultra-high resistivity substrate of $\rho_{Si} > 10^4$–$10^5\ \Omega$ cm was realized through proton bombardment to effectively raise Q by around 100% but keep nearly nothing change to f_{SR}. Regarding the very low resistivity region of $\rho_{Si} < 0.5\ \Omega$ cm, f_{SR} saturates at a minimum and Q_m drops drastically. The spiral coil is driven into an eddy current mode or skin effect mode where ρ_{Si} is so small that the skin depth is thinner than the substrate thickness and becomes the limiting factor.

2.3. Analytical models for f_{SR} under varying substrate resistivities

The interesting results of f_{SR} under varying ρ_{Si} trigger our motivation to derive analytical models for prediction of f_{SR}. The ultimate goal is a close form as an explicit function of physical parameters without resort to EM simulation. Firstly, equivalent circuit analysis was performed on our T-model through circuit conversion shown in Fig. 5 under an appropriate approximation to simplify the circuit topology and yield a closed form for f_{SR} with sufficient accuracy. The approximation made by removing the eddy current elements such as $L_{sub\ 1,2}$, $R_{loss1,2}$, L_{sub}, and R_{loss} leading to so call reduced T-model was justified by an impedance analysis and equivalent circuit simulation. Fig. 6 presents $Q(\omega)$ calculated by the reduced T-model without eddy current terms and the comparison with the original T-model. The major difference is revealed in higher frequency region beyond the Q_m but the intercept point corresponding to $Q = 0$, i.e. the self-resonance frequency f_{SR} is nearly identical to each other.

In the following, the model equations for calculating f_{SR} under varying ρ_{Si} can be readily derived based on the validated reduced T-model circuit topology in Fig. 5.

To calculate the impedance Z_{in} from $Z_{in} = 1/Y_{in}$,

$$Y_{in} = \frac{1}{Z_1} + \frac{1}{Z_2 + \frac{Z_3 \times Z_4}{Z_3 + Z_4}}$$

$$= \frac{1}{R_p} + sC_p + \frac{1}{R_s + sL_s} + \frac{sC_{ox1} + s^2 R_{sub} C_{ox1}(C_{sub} + C_{ox2})}{1 + sR_{sub}(C_{ox1} + C_{ox2} + C_{sub})} \quad (1)$$
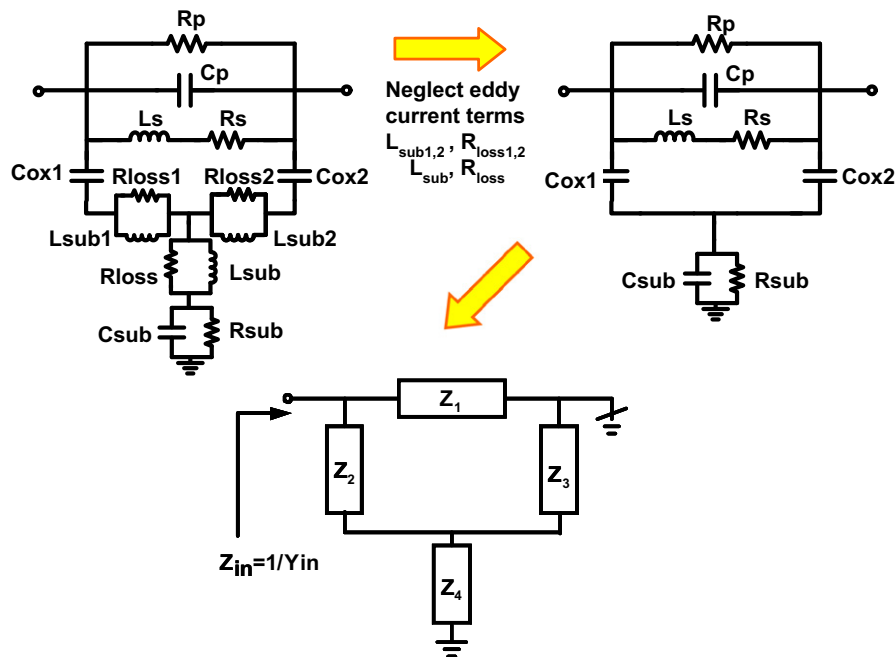

Fig. 6. Comparison of $Q(\omega)$ and self-resonance frequency f_{SR} corresponding to $Q = 0$ among original T-model, reduced T-model ($L_{sub\ 1,2} = R_{loss1,2} = L_{sub} = R_{loss} = 0$) and measurement for spiral inductors with various coil numbers, $N = 2.5$, 3.5, 4.5, and 5.5.

Define

$$s = j\omega$$
$$C_T = C_{ox1} + C_{ox2} + C_{sub} \quad (2)$$

Then

$$Y_{in} = \frac{1}{R_p} + \frac{1}{R_s} + \frac{1}{1 + \left(\frac{\omega L_s}{R_s}\right)^2} + \frac{\omega^2 R_{sub} C_{ox1}^2}{1 + (\omega R_{sub} C_T)^2}$$

$$+ j\omega C_p - j\frac{1}{R_s^2}\frac{\omega L_s}{1 + \left(\frac{\omega L_s}{R_s}\right)^2} + j\frac{\omega C_{ox1} + \omega^3 R_{sub}^2 C_{ox1} C_T (C_{sub} + C_{ox2})}{1 + (\omega R_{sub} C_T)^2}$$

$$(3)$$

Fig. 5. Equivalent circuit schematics and analysis of reduced T-model to derive the analytical models for calculating self-resonance frequency f_{SR}.
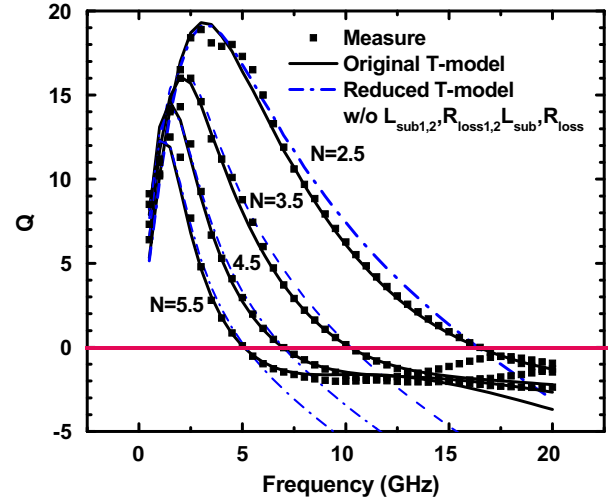
∴the quality factor Q can be derived as follows

$$Q = \frac{\text{Im}(1/Y_{\text{in}})}{\text{Re}(1/Y_{\text{in}})} = \frac{\omega C_{\text{p}} - \frac{1}{R_{\text{s}}^2}\frac{\omega L_{\text{s}}}{\left(\frac{\omega L_{\text{s}}}{R_{\text{s}}}\right)^2} + \frac{\omega C_{\text{ox1}} + \omega^3 R_{\text{sub}}^2 C_{\text{ox1}} C_{\text{T}}(C_{\text{sub}}+C_{\text{ox2}})}{1+(\omega R_{\text{sub}}C_{\text{T}})^2}}{\frac{1}{R_{\text{p}}} + \frac{1}{R_{\text{s}}}\frac{1}{1+(\frac{\omega L_{\text{s}}}{R_{\text{s}}})^2} + \frac{\omega^2 R_{\text{sub}}^2 C_{\text{ox1}}^2}{1+(\omega R_{\text{sub}}C_{\text{T}})^2}} \tag{4}$$

The self-resonance frequency, $\omega_{\text{SR}} = 2\pi f_{\text{SR}}$ is derived corresponding to $Q = 0$

$$Q(\omega = \omega_{\text{SR}}) = 0 \Rightarrow \text{Im}(1/Y_{\text{in}}(\omega))|_{\omega=\omega_{\text{SR}}} = 0 \tag{5}$$

$$\omega C_{\text{p}} - \frac{1}{R_{\text{s}}^2}\frac{\omega L_{\text{s}}}{1+(\frac{\omega L_{\text{s}}}{R_{\text{s}}})^2} + \frac{\omega C_{\text{ox1}}[1+\omega^2 R_{\text{sub}}^2 C_{\text{T}}(C_{\text{sub}}+C_{\text{ox2}})]}{1+(\omega R_{\text{sub}}C_{\text{T}})^2}\Bigg|_{\omega=\omega_{\text{SR}}} = 0 \tag{6}$$

For operation in TEM mode, i.e.

$\rho_{\text{Si}} \geqslant 10\,\Omega\,\text{cm} \Rightarrow R_{\text{sub}} \gg 100\,\Omega$

$$\omega \to \omega_{\text{SR}} : (\omega R_{\text{sub}}C_{\text{T}})^2 \gg 1 \to 1+(\omega R_{\text{sub}}C_{\text{T}})^2 \approx (\omega R_{\text{sub}}C_{\text{T}})^2 \tag{7}$$

$$\omega \to \omega_{\text{SR}} : \omega^2 R_{\text{sub}}^2 C_{\text{T}}(C_{\text{sub}}+C_{\text{ox2}}) \gg 1$$
$$\therefore 1+\omega^2 R_{\text{sub}}^2 C_{\text{T}}(C_{\text{sub}}+C_{\text{ox2}}) \approx \omega^2 R_{\text{sub}}^2 C_{\text{T}}(C_{\text{sub}}+C_{\text{ox2}}) \tag{8}$$

$$\omega \to \omega_{\text{SR}} : \left(\frac{\omega L_{\text{s}}}{R_{\text{s}}}\right)^2 \gg 1 \to 1+\left(\frac{\omega L_{\text{s}}}{R_{\text{s}}}\right)^2 \approx \left(\frac{\omega L_{\text{s}}}{R_{\text{s}}}\right)^2 \tag{9}$$

under the approximation (7), (8) and (9), (6) can be simplified as follows:

$$\omega C_{\text{p}} - \frac{1}{R_{\text{s}}^2}\frac{\omega L_{\text{s}}}{1+\left(\frac{\omega L_{\text{s}}}{R_{\text{s}}}\right)^2} + \frac{\omega C_{\text{ox1}}+\omega^3 R_{\text{sub}}^2 C_{\text{ox1}} C_{\text{T}}(C_{\text{sub}}+C_{\text{ox2}})}{1+(\omega R_{\text{sub}}C_{\text{T}})^2}|_{\omega=\omega_{\text{SR}}} = 0$$

$$\Rightarrow \omega^2\left(\frac{C_{\text{ox1}}(C_{\text{sub}}+C_{\text{ox2}})}{C_{\text{T}}} + C_{\text{p}}\right)\Bigg|_{\omega=\omega_{\text{SR}}} = \frac{1}{L_{\text{s}}} \tag{10}$$

$$\Rightarrow \omega_{\text{SR}} = \sqrt{\frac{1}{L_{\text{s}}}\times\left(\frac{C_{\text{ox1}}+C_{\text{ox2}}+C_{\text{sub}}}{C_{\text{p}}(C_{\text{ox1}}+C_{\text{ox2}}+C_{\text{sub}})+C_{\text{ox1}}(C_{\text{sub}}+C_{\text{ox2}})}\right)} \tag{11}$$

$$\therefore f_{\text{SR}} = \frac{1}{2\pi}\sqrt{\frac{1}{L_{\text{s}}}*\left(\frac{C_{\text{ox1}}+C_{\text{ox2}}+C_{\text{sub}}}{C_{\text{p}}(C_{\text{ox1}}+C_{\text{ox2}}+C_{\text{sub}})+C_{\text{ox1}}(C_{\text{sub}}+C_{\text{ox2}})}\right)} \tag{12}$$

For operation in eddy current mode, i.e.

$\rho_{\text{Si}} \leqslant 0.5\,\Omega\,\text{cm} \Rightarrow R_{\text{sub}} \ll 2\,\Omega$

$$\omega \to \omega_{\text{SR}} : (\omega R_{\text{sub}}C_{\text{T}})^2 \ll 1 \to 1+(\omega R_{\text{sub}}C_{\text{T}})^2 \approx 1 \tag{13}$$

$$\omega \to \omega_{\text{SR}} : \omega^2 R_{\text{sub}}^2 C_{\text{T}}(C_{\text{sub}}+C_{\text{ox2}}) \ll 1$$
$$\to 1+\omega^2 R_{\text{sub}}^2 C_{\text{T}}(C_{\text{sub}}+C_{\text{ox2}}) \approx 1 \tag{14}$$

$$\therefore \frac{\omega C_{\text{ox1}}[1+\omega^2 R_{\text{sub}}^2 C_{\text{T}}(C_{\text{sub}}+C_{\text{ox2}})]}{1+(\omega R_{\text{sub}}C_{\text{T}})^2}\Bigg|_{\omega=\omega_{\text{SR}}} \cong \omega C_{\text{ox1}} \tag{15}$$

According to (13)–(15), $\text{Im}(1/Y_{\text{in}})$ in (4) can be approximated by

$$\text{Im}(1/Y_{\text{in}}) \cong \omega C_{\text{p}} - \frac{1}{R_{\text{s}}^2}\frac{\omega L_{\text{s}}}{1+\left(\frac{\omega L_{\text{s}}}{R_{\text{s}}}\right)^2} + \omega C_{\text{ox1}} \tag{16}$$

$$Q(\omega = \omega_{\text{SR}}) = 0 \to \text{Im}(1/Y_{\text{in}})|_{\omega=\omega_{\text{SR}}} = 0$$

$$\omega C_{\text{p}} - \frac{1}{R_{\text{s}}^2}\frac{\omega L_{\text{s}}}{1+\left(\frac{\omega L_{\text{s}}}{R_{\text{s}}}\right)^2} + \omega C_{\text{ox1}}|_{\omega=\omega_{\text{SR}}} = 0$$

$$\Rightarrow \omega_{\text{SR}}^2 + (R_{\text{s}}/L_{\text{s}})^2 = \frac{1}{L_{\text{s}}(C_{\text{p}}+C_{\text{ox1}})}$$

$$\Rightarrow \omega_{\text{SR}} = \sqrt{\frac{1}{L_{\text{s}}(C_{\text{p}}+C_{\text{ox1}})} - (R_{\text{s}}/L_{\text{s}})^2} \tag{17}$$

$$\therefore f_{\text{SR}} = \frac{1}{2\pi}\sqrt{\frac{1}{L_{\text{s}}(C_{\text{p}}+C_{\text{ox1}})} - (R_{\text{s}}/L_{\text{s}})^2} \tag{18}$$

As a result, the self-resonance frequency f_{SR} in TEM mode with sufficiently high substrate resistivity, $\rho_{\text{Si}} > 10\,\Omega$ cm can be calculated in a simple equation given by (12) while f_{SR} in eddy current mode with very low substrate resistivity, $\rho_{\text{Si}} < 0.5\,\Omega$ cm can be predicted by (18). Note that both (12) and (18) are independent of ρ_{Si}, which is consistent with EM simulation results shown in Fig. 4b. The accuracy of f_{SR} calculated by the simple model equations was seriously verified through an extensive comparison with EM simulation results. Table 1 indicates a good agreement between the analytical model and EM simulation for both TEM mode ($\rho_{\text{Si}} = 10$–$1000\,\Omega$ cm) and eddy current mode ($\rho_{\text{Si}} = 0.05$–$1\,\Omega$ cm). Besides, the approximations made in (7) and (13) for $(\omega_{\text{SR}}R_{\text{sub}}C_{\text{T}})^2$ are justified by R_{sub}, C_{T}, and f_{SR} ($\omega_{\text{SR}} = 2\pi f_{\text{SR}}$) in the table to validate the simplification of (6) and derivation of a simple close form. The analytical models with proven accuracy are useful in guiding on-chip inductor design for f_{SR} improvement. For an operation in TEM mode, f_{SR} can be enhanced by reducing L_{s} and all parasitic capacitances in spiral coil as well as substrate networks, such as C_{p}, $C_{\text{ox1,2}}$, and C_{sub}. As for eddy current mode, f_{SR} can be improved by reducing L_{s} as well as R_{s} simultaneously, and parasitic capacitances in spiral coil network and inter-network coupling path, i.e. C_{p} and $C_{\text{ox1,2}}$. Note that f_{SR} in the eddy current mode is independent of substrate network element like C_{sub} while that in TEM mode is independent of R_{s}. Furthermore, the analytical models predict that f_{SR} in the eddy current mode is always lower than that in TEM mode with an only exception that $C_{\text{ox1,2}}$ and R_{s} can be eliminated simultaneously.

Table 1
The self-resonance frequency f_{SR} calculated by analytical model equations for TEM mode and eddy current modes corresponding to very high and very low substrate resistivities ($\rho_{\text{Si}} = 0.05$–1 KΩ cm)

Operation modes	ρ_{Si} (Ω cm)	R_{sub}(Ω)	C_{T} (fF)	$(\omega_{\text{SR}}R_{\text{sub}}C_{\text{T}})^2$	f_{SR} (GHz)	
					EM simulation	Analytical model
Eddy current mode (skin effect)	0.05	0.134	393.097	1.851E−05	13	11.785
	0.1	0.91	396.694	8.561E−04	12.9	11.577
	0.5	1.82	366.745	2.927E−03	12.9	12.699
Slow-wave mode (resonator)	1	3.87	345.650	0.012	13.2	13.524
	2.5	28.30	294.064	0.591	14.7	–
	5	54.35	263.748	2.077	16	–
	7.5	113.64	228.940	7.275	16.5	–
TEM mode (inductor)	10	138.75	227.176	10.939	16.7	16.102
	50	797	188.030	253.224	16.9	16.854
	100	1513	179.981	845.708	17	16.987
	1000	6296	179.981	14650.101	17	16.987

The comparison with those predicted by EM simulation using calibrated ADS momentum indicates good agreement and justifies the accuracy of the analytical models. R_{sub}, C_{T}, and $(\omega_{\text{SR}}R_{\text{sub}}C_{\text{T}})^2$ shown in the table validates the approximation made for deriving the equations of close form.

2.4. T-model scalability over inductor geometries and substrate resistivities

One more important feature, which is offered from our T-model and makes the derived analytical model for f_{SR} more powerful is the scalability over inductor geometries and substrate resistivities ρ_{Si}. All of the circuit elements in our proprietary T-model are frequency independent and scalable over inductor geometries, such as spiral coil numbers (N) and metal trace width (W). The scalability can be well modeled as a simple linear or parabolic function [9]. Moreover, all the model parameters manifest themselves as physics-based through a relevant correlation with ρ_{Si} in three operation modes. Herein, R_{sub} in the substrate network, playing as an element most strongly correlated with ρ_{Si} is selected for validating the scalability. Fig. 7a and b demonstrate $1/R_{sub}$ versus coil number (N) and metal trace width (W), which match very well a linear function of N and a parabolic function of W, respectively. A comprehensive result involving all model parameters over various N and W can be referred to our original work [9]. Regarding ρ_{Si} effect of our special interest in this study, R_{sub} versus ρ_{Si} covering all three operation modes is presented in Fig. 8. The result indicates a simple function of $R_{sub} = 7.0164 \times \rho_{Si}^{1.1163}$ in which R_{sub} is proportional to ρ_{Si} with a power law approaching unity. Based on the individual scalable model with an expression of mathematical formulas as a function of N, W, and ρ_{Si}, respectively, a comprehensive scalable model incorporating all three variables (N, W, ρ_{Si}) can be derived as shown in (19)–(20). The derived scalable model in a simple explicit function makes the analytical model very useful in inductor design and RF circuit simulation.

Analytical model for R_{sub} as a function of N, W, and ρ_{Si}

$$R_{sub} = \frac{A_0 \rho_{Si}^{\beta}}{(N + A_1)(W^2 + A_2 W + A_3)} \qquad (19)$$

where

ρ_{Si}: substrate resistivity in the unit of Ω cm
N: spiral coil number
W: spiral metal trace width in the unit of μm

$$\beta = 1.1163 \qquad (20.1)$$
$$A_0 = 1.232 \times 10^4 \qquad (20.2)$$
$$A_1 = -0.798 \qquad (20.3)$$
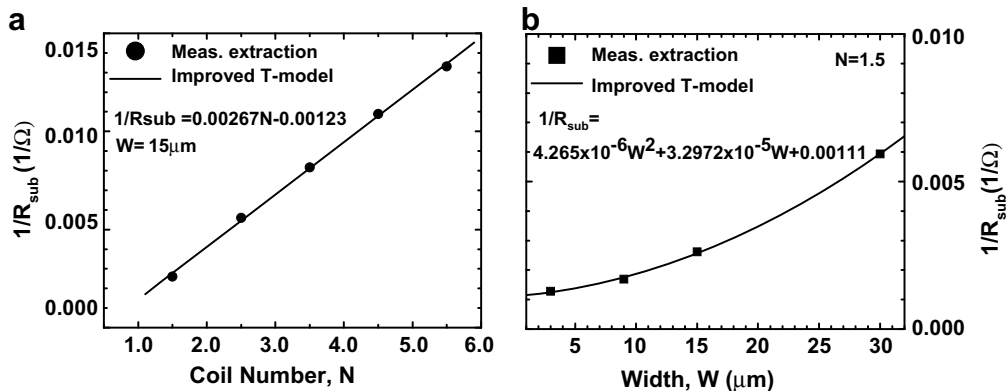$$A_2 = 7.731 \qquad (20.4)$$
$$A_3 = 260.27 \qquad (20.5)$$

Fig. 8. T-model parameter R_{sub} as a function of substrate resistivity ρ_{Si}, which can be fitted by a simple power law function of $R_{sub} = 7.0164 \times \rho_{Si}^{1.1163}$.

3. Conclusions

A simple analytical model in the form of explicit formulas have been derived to accurately calculate f_{SR} of on-chip spiral inductors operating in TEM and eddy current modes. For an operation in TEM mode, f_{SR} is determined by the inductance L_s and all parasitic capacitive elements adopted in the T-model such as C_p, $C_{ox1,2}$, and C_{sub} but is independent of coil metal parasitic resistance R_S. As for eddy current mode, f_{SR} depends on both L_s and R_s of the spiral coil, and three parasitic capacitances C_p and $C_{ox\ 1,2}$, but is independent of the substrate network capacitance, C_{sub}. This simple analytical model is useful to guide on-silicon-chip inductor design for increasing f_{SR} under specified inductance aimed for broadband RF circuit design and applications.

Fig. 7. T-model parameter R_{sub} as a function of coil number and metal trace width: (a) $1/R_{sub}$ vs. N, fitted by $1/R_{sub} = 0.00267N - 0.00123$; (b) $1/R_{sub}$ vs. W, $1/R_{sub} = 4.265 \times 10^{-6}W^2 + 3.2972 \times 10^{-5}W + 0.00111$.
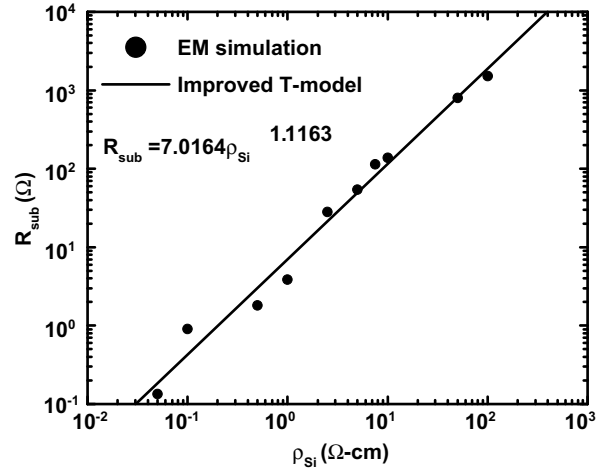
References

[1] Burghartz JN, Edelstein DC, Soyuer M, Ainspan HA, Jenkins KA. RF circuit design aspects of spiral inductors on silicon. IEEE J Solid-State Circ 1998;33: 2028–34.

[2] Burghartz JN, Rejaei B. On the design of RF spiral inductors on silicon. IEEE Trans Electron Dev 2003;50:718–29.

[3] Burghartz JN, Edelstein DC, Jenkiin KA, Kwark YH. Spiral inductors and transmission lines in silicon technology using copper-damascene interconnects and low-loss substrates. IEEE Trans Microwave Theor Tech 1997;45:1961–8.

[4] Lakdawala H, Zhu X, Luo H, Santhanam S, Carley LR, Fedder GK. Micromachined high-Q inductors in a 0.18-µm copper interconnect low-*k* dielectric CMOS process. IEEE J Solid-State Circ 2002;37:394–403.

[5] Royet AS, Cuchet R, Pellissier D, Ancey P. On the investigation of spiral inductors processed on Si substrates with thick porous Si layers. In: ESSDERC proceedings; 2003. p. 111–4.

[6] Tang DD, Lin WC, Lai LS, Wang CH, Lee LP, Hsu HM, et al. The integration of proton bombardment process into the manufacturing of mixed-signal/RF chips. In: IEDM tech. digest; 2003. p. 673–6.

[7] Yue CP, Wong SS. On-chip spiral inductors with patterned ground shields for Si-based RF ICs. IEEE J Solid-State Circ 1998;33:743–52.

[8] Cheung TSD, Long JR, Vaed K, Volant R, Chinthakindi A, Schnabel CMJ, et al. Differentially-shielded monolithic inductors. In: IEEE CiCC Proceedings; 2003. p. 95–8.

[9] Guo Jyh-Chyurn, Tan Teng-Yang. A broadband and scalable on-chip inductor model appropriate for operation modes of varying substrate resistivities. IEEE Trans Electron Dev 2007;54:3018–29.

[10] Hasegawa H, Furukawa M, Yanai H. Properties of microstrip line on Si–SiO$_2$ system. IEEE Trans Microwave Theor Tech 1971;19:869–81.

[11] Yue CP, Wong SS. Physical modeling of spiral inductors on silicon. IEEE Trans Electron Dev 2000;47:560–8.

[12] Park M, Lee S, Kim CS, Yu HK, Nam KS. The detailed analysis of high Q CMOS-compatible microwave spiral inductors in silicon technology. IEEE Trans Electron Dev 1998;45:1953–9.

[13] Cao Yu, Grove RA, Huang X, Zamdmer ND, Plouchart J-O, Wachnik RA, et al. Frequency-independent equivalent-circuit model for on-chip spiral inductors. IEEE J Solid-State Circ 2003;38:419–26.

[14] Fujishima M, Kino J. Accurate subcircuit model of an on-chip inductor with a new substrate network. In: VLSI symp digest; 2004. p. 376–9.

[15] Gil J, Shin H. A simple wide-band on-chip inductor model for silicon-based RF Ics. IEEE Trans Microwave Theor Tech 2003;51(Sept):2023–8.

[16] B, Tauritz JL, Snoeij P. A predictive model for Si-based circular spiral inductors. In: IEEE silicon monolithic integrated circuits in RF systems meeting, Ann Arbor; 1998. p. 148–54.